

## Research Paper

# Placenta-specific drug delivery by trophoblast-targeted nanoparticles in mice

Baozhen Zhang<sup>1\*</sup>, Lunbo Tan<sup>1,2\*</sup>, Yan Yu<sup>3\*</sup>, Baobei Wang<sup>1</sup>, Zhilong Chen<sup>1,2</sup>, Jinyu Han<sup>1</sup>, Mengxia Li<sup>1</sup>, Jie Chen<sup>1</sup>, Tianxia Xiao<sup>1</sup>, Balamurali K Ambati<sup>4</sup>, Lintao Cai<sup>5</sup>, Qing Yang<sup>2</sup>, Nihar R Nayak<sup>6</sup>, Jian Zhang<sup>1</sup>, Xiujun Fan<sup>1</sup>

1. Laboratory for Reproductive Health, Institute of Biomedicine and Biotechnology, Shenzhen Institutes of Advanced Technology (SIAT), Chinese Academy of Sciences (CAS), Shenzhen, Guangdong, China, 518055.
2. College of Veterinary Medicine, Hunan Agricultural University, Changsha, Hunan, China, 410128.
3. Bao'an Maternal and Child Health Care Hospital, Shenzhen, China, 518133.
4. John A. Moran Eye Center, University of Utah, Salt Lake City, Utah, USA, 84132.
5. Guangdong Key Laboratory of Nanomedicine, CAS Key Lab for Health Informatics, Institute of Biomedicine and Biotechnology, Shenzhen Institutes of Advanced Technology, Chinese Academy of Sciences, Shenzhen, China, 518055.
6. Department of Obstetrics and Gynecology, Wayne State University School of Medicine, C.S. Mott Center for Human Growth and Development, Detroit, Michigan, USA, 48201.

\* Contributed equally to this work

 Corresponding author: Xiujun Fan, E-mail: xj.fan@siat.ac.cn, Phone: 86 755 86392360. Fax: 86 755 86392282. Jian Zhang, E-mail: jian.zhang@siat.ac.cn, Nihar R. Nayak, E-mail: nnayak@med.wayne.edu.

© Ivyspring International Publisher. This is an open access article distributed under the terms of the Creative Commons Attribution (CC BY-NC) license (<https://creativecommons.org/licenses/by-nc/4.0/>). See <http://ivyspring.com/terms> for full terms and conditions.

Received: 2017.09.20; Accepted: 2018.02.09; Published: 2018.04.09

## Abstract

**Rationale:** The availability of therapeutics to treat pregnancy complications is severely lacking, mainly due to the risk of harm to the fetus. In placental malaria, *Plasmodium falciparum*-infected erythrocytes (IEs) accumulate in the placenta by adhering to chondroitin sulfate A (CSA) on the surfaces of trophoblasts. Based on this principle, we have developed a method for targeted delivery of payloads to the placenta using a synthetic placental CSA-binding peptide (pICSA-BP) derived from VAR2CSA, a CSA-binding protein expressed on IEs.

**Methods:** A biotinylated pICSA-BP was used to examine the specificity of pICSA-BP binding to mouse and human placental tissue in tissue sections *in vitro*. Different nanoparticles, including pICSA-BP-conjugated nanoparticles loaded with indocyanine green (pICSA-INPs) or methotrexate (pICSA-MNPs), were administered intravenously to pregnant mice to test their efficiency at drug delivery to the placenta *in vivo*. The tissue distribution and localization of the pICSA-INPs were monitored in live animals using an IVIS imaging system. The effect of pICSA-MNPs on fetal and placental development and pregnancy outcome were examined using a small-animal high-frequency ultrasound (HFUS) imaging system, and the concentrations of methotrexate in fetal and placental tissues were measured using high-performance liquid chromatography (HPLC).

**Results:** pICSA-BP binds specifically to trophoblasts and not to other cell types in the placenta or to CSA-expressing cells in other tissues. Moreover, we found that intravenously administered pICSA-INPs accumulate in the mouse placenta, and *ex vivo* analysis of the fetuses and placentas confirmed placenta-specific delivery of these nanoparticles. We also demonstrate successful delivery of methotrexate specifically to placental cells by pICSA-BP-conjugated nanoparticles, resulting in dramatic impairment of placental and fetal development. Importantly, pICSA-MNPs treatment had no apparent adverse effects on maternal tissues.

**Conclusion:** These results demonstrate that pICSA-BP-guided nanoparticles could be used for the targeted delivery of payloads to the placenta and serve as a novel placenta-specific drug delivery option.

Key words: trophoblast, chondroitin sulfate A, placental CSA binding peptide, nanoparticles

## Introduction

Pregnancy complications, including pre-eclampsia, fetal growth restriction, preterm birth, placental abruption, and late pregnancy loss, are common, affecting more than 1 in 6 pregnancies, and

lead to substantial maternal, fetal, and neonatal morbidity and mortality [1-3]. The causes of these complications remain unclear, but it has been postulated that placental insufficiency plays a primary role in each case [1].

Currently, there are no effective preventive strategies for these disorders: only a few drugs have been licensed for pregnancy disorders over the last two decades [4, 5], and the efficacy of existing therapeutic agents is extremely limited. Moreover, these agents are small molecules with low molecular weights and readily cross the placenta from mother to fetus, often leading to serious fetal side effects [6]. Minimizing fetal exposure to medication is a major challenge in developing safer medications to treat pregnancy complications.

Nanomedicine is a multidisciplinary field of medicine and nanotechnology that seeks to increase the safety and efficacy of drugs by directing them preferentially to specific tissues [7], and it has opened up opportunities for novel modalities for the delivery of drugs in pregnancy [8-10]. Recently, we developed a well-defined lipid-polymer nanoparticle (NP) platform using a fast single-step sonication method that allows control of particle size and surface functionalities, and has demonstrated good monodispersity, high drug-loading capability, sustained drug release, and excellent *in vitro* and *in vivo* stability [11, 12]. Importantly, toxicity studies in mice indicate that these nanoparticles are well tolerated, with no adverse side effects [11, 12].

Chondroitin sulfate A (CSA) is present on placental syncytiotrophoblasts and plays a key role in malarial pathogenesis. The malaria parasite *Plasmodium falciparum* has evolved a protein, VAR2CSA, that mediates the binding of infected erythrocytes (IEs) to a distinct type of CSA present on placental syncytiotrophoblasts [13, 14]. The minimal CSA-binding region of VAR2CSA consists of the Duffy Binding Ligand-like (DBL) 2X domain along with flanking interdomain (ID) regions [15, 16]. Phage screening identified a peptide from the DBL2X domain that selectively binds to CSA [17]; we named this synthetic peptide placental CSA binding peptide (pLCSA-BP).

Given this background, we were interested in whether synthetic pLCSA-BP conjugation to our lipid-polymer nanoparticle could effectively target delivery of payloads to the placenta. Here, we describe the successful fabrication of a pLCSA-NP that was able to deliver methotrexate (MTX), an antifolate agent used to treat ectopic pregnancy and choriocarcinoma [18-20], specifically to mouse placental trophoblasts *in vitro*, *ex vivo*, and *in vivo*. We demonstrate that pLCSA-BP can be exploited for the

targeted delivery of drugs to the placenta.

## Methods

### Materials

Soybean lecithin and 1,2-distearoyl-*sn*-glycero-3-phosphoethanolamine-N-maleimide (polyethylene glycol 2000) carboxylic acid (DSPE-PEG-COOH) were purchased from Avanti Polar Lipids (Alabama, USA). Poly (lactide-*co*-glycolide) (PLGA), 1-ethyl-3-(3-dimethylaminopropyl) carbodiimide hydrochloride (EDC), *N*-hydroxysuccinimide (NHS), methotrexate (MTX) and indocyanine green (ICG) were obtained from Sigma-Aldrich (Missouri, USA). Unless stated otherwise, all other materials used were purchased from Sigma-Aldrich (Missouri, USA). Placental CSA-binding peptide (pLCSA-BP, EDVKDINFDTKEK FLAGCLIVSFHEGKC) and N-terminal  $\alpha$ -amino-biotinylated pLCSA-BP (biotin-pLCSA-BP) were purchased from ChinaPeptides Co.,Ltd. (Shanghai, China). The scrambled peptide (SCR, EVDNDKKLGL VFEKDKIFTEFACISHCG) and N-terminal  $\alpha$ -amino-biotinylated SCR (biotin-SCR) were synthesized at Shanghai GL Biochem Co., Ltd. (Shanghai, China).

### Synthesis of pLCSA-BP-conjugated nanoparticles and SCR-conjugated nanoparticles

Lipid-polymer nanoparticles (NPs) loaded with MTX (MNPs) were synthesized from PLGA, soybean lecithin, MTX and DSPE-PEG-COOH using our previously published single-step sonication method [11]. The peptides were conjugated to DSPE-PEG-COOH using EDC and NHS, as follows. First, 18 mg of the MNPs was suspended in 6mL of 0.1M 2-morpholinoethanesulfonic acid (MES) buffer (pH 5.5). To pre-activate the carboxylic group, 15 mg of EDC and 5 mg of NHS were added, and the mixture was stirred for 15 min at room temperature. 3 mg of pLCSA-BP or SCR was then dissolved in 500  $\mu$ L of deionized water and the solution was added to the reaction mixture separately. Next, 350  $\mu$ L of 20 $\times$  phosphate-buffered saline (PBS) was added to buffer the reaction, which was maintained at pH 7.0-8.0. The reaction mixture was then stirred overnight at room temperature. Excess peptide and other impurities, such as EDC and NHS, were removed by triple filtration using AmiconUltra-4 centrifugal filters (MW10kD, Millipore, MA, USA) to obtain final pLCSA-BP-conjugated nanoparticles loaded with MTX (pLCSA-MNPs) and SCR-conjugated nanoparticles loaded with MTX (SCR-MNPs). The same procedures were used to prepare the pLCSA-BP-conjugated nanoparticles loaded with indocyanine green (ICG, pLCSA-INPs) and SCR-conjugated nanoparticles

loaded with ICG (SCR-INPs).

Conjugation efficiencies were determined using a bicinchoninic acid (BCA) assay. Briefly, 200  $\mu$ L of BCA assay reagent (50:1, BCA:CuSO<sub>4</sub>) was added to wells in a 96-well plate, followed by 25  $\mu$ L of pICSA-NPs or SCR-NPs. The mixtures were further incubated for 30 min at 37°C, and fluorescence was measured at 562 nm with a microplate reader (Thermo Fisher, USA).

### Characterization of the nanoparticles

The size, polydispersity, and surface charge of the nanoparticles were determined using a Beckman Coulter Delsa TM Nano C (Beckman, USA) at room temperature. Nanoparticle morphology and size were visualized using transmission electron microscopy (TEM, JEM-100CXII). Briefly, nanoparticles suspensions (0.1 mg/mL) were loaded onto carbon-coated copper grids for 5 min, and excess liquid was removed with filter paper. The grids were then stained with 2% (w/v) phosphotungstic acid for 1 min and dried at room temperature before image acquisition.

To determine encapsulation efficiency (EE) and drug loading efficiency (LE) for MTX in the nanoparticles, before ultrafiltration, newly synthesized nanoparticles were isolated from the aqueous suspensions using a Beckman Optima TM MAX-XP ultracentrifuge (34,000 $\times$ g, 30 min) (Beckman, USA). The non-entrapped MTX in the supernatant was quantified using fluorescence spectroscopy (F900, Edinburgh Instruments Ltd., UK) with emission at 545 nm and excitation at 300 nm. The EE and LE were calculated as follows:  $EE = ((\text{weight of loaded MTX}) / (\text{weight of initially added MTX})) \times 100\%$ , and  $LE = ((\text{weight of loaded MTX}) / (\text{total weight of NPs})) \times 100\%$ .

A dialysis experiment was performed to measure MTX release from different MTX formulations, with PBS (pH 7.4) as the release medium. Different MTX formulations (100  $\mu$ g MTX equivalent) dispersed in 1 mL of release medium were added to dialysis bags (MWCO, 3500 Da, Bestbio, Shanghai, China), and the bags were incubated in 100 mL of the same medium at 37°C on a rotator at 120 rpm. At predetermined time points, the dialysate was removed to measure drug release, and an equal volume of fresh PBS was added. MTX concentrations in the dialysates were measured by fluorescence spectroscopy with emission at 545 nm and excitation at 300 nm. The *in vitro* stabilities of different nanoparticles were investigated by dispersing the nanoparticles in 10% fetal bovine serum (FBS) and examining changes in size.

### Animals

CD1 mice (6-8 weeks of age) were obtained from Beijing Vital River Laboratory Animal Technology Co., Ltd. (Beijing, China) and caged in a specific pathogen-free animal room with a 14 h light/10 h dark cycle. Gestational ages were determined by monitoring formation of vaginal plugs (E0.5=vaginal plug day) and confirmed by measuring gestational sac lengths using an ultrasound imaging system. Pregnant mice were injected intravenously in the tail vein with free MTX, MNPs, SCR-MNPs, or pICSA-MNPs at an MTX equivalent dose of 1 mg/kg every second day starting at E6.5.

### Immunofluorescence

Mice were anesthetized with 30% urethane. After cardiac perfusion with PBS, tissues were removed and fixed in 4% paraformaldehyde (PFA) overnight. After dehydration in 30% sucrose, tissues were embedded in OCT and frozen, and tissue blocks were stored at -80°C until sectioning. 10  $\mu$ m serial sections were obtained for immunostaining. After blocking tissue sections with bovine serum albumin (BSA), sections were incubated with biotin-pICSA-BP (50 ng/mL), biotin-SCR (50 ng/mL) or primary antibodies overnight at 4°C as follows: rat monoclonal anti-CD31 (1:200; BD Pharmingen, CA, USA); rat monoclonal anti-cytokeratin 8 (CK8; 1:100; National Institutes of Health Developmental Studies Hybridoma Bank, Iowa, USA); or mouse monoclonal anti-C4S (2B6, 1:20; Amsbio, UK). Tissue sections were then washed 3 times (TBS, 5 min) and incubated at room temperature with Alexa 488-donkey anti-rat (1:200; Thermo Fisher Scientific, MA, USA), Alexa 594-donkey anti-rat (1:200; Thermo Fisher Scientific, MA, USA), or Alexa 594-goat anti-mouse (1:200; Thermo Fisher Scientific, MA, USA) secondary antibody or FITC-avidin (1:64; Boster, Wuhan, China) separately for 30 min. Stained sections were mounted using mounting medium containing DAPI (Vector Laboratories, CA, USA) and examined using fluorescence microscopy (Olympus, Japan) and confocal microscopy (Leica, TCS SP5, Germany).

### Immunohistochemistry

Normal human placental villous tissues were collected after informed consent from elective terminations according to an IRB approved protocol at the Bao'an Maternal and Child Health Care Hospital of Shenzhen, described below. Immunohistochemistry (IHC) was performed according to our previously published procedures [21]. Briefly, human and mouse tissue sections (5  $\mu$ m) were deparaffinized and rehydrated. Slides were then microwaved in antigen retrieval buffer (0.01 M sodium citrate,

pH 6.0). After cooling, slides were incubated with hydrogen peroxide (3% w/v) for 20 min to inactive endogenous peroxidases, washed in TBS, and incubated with BSA for 30 min. Sections were then incubated with biotin-pICSA-BP (50 ng/mL), biotin-SCR (50 ng/mL), mouse monoclonal anti-C4S antibody (2B6, 1:20; Amsbio, UK), or control IgG (Abcam, UK) overnight at 4°C. Tissue sections were then washed and incubated with HRP-donkey anti-mouse IgG (1:200; Thermo Fisher Scientific, USA) or HRP-streptavidin (1:200; Boster, Wuhan, China). Hematoxylin (blue) was used as a counter-stain. Staining was visualized on a light microscope (Olympus BX53, Japan).

## H&E

Tissue collection and processing for histological analysis were performed following a standard protocol, as described previously by us and others [22, 23]. Briefly, tissue samples from placentas, livers, and kidneys were collected and fixed in 4% PFA overnight at 4°C. Subsequently, the tissues were infiltrated with and embedded in paraffin, sectioned, stained with H&E, and examined on a light microscope (Olympus BX53, Japan).

## Ultrasonographic measurements of embryo development

Mice were anesthetized with 5% isoflurane at 1 L of O<sub>2</sub>/min and maintained under 3% isoflurane in 1 L of O<sub>2</sub>/min for the duration of the scan. The mice were kept warm on a heated platform (37°C) connected to a temperature/physiology monitor. Embryo development was monitored using a dedicated small-animal high-frequency ultrasound (HFUS) imaging system (Vevo 2100; VisualSonics, Toronto, Canada) with ultrasound settings standardized as follows: frequency, 40 MHz; power, 100%; and gain, 30 dB. Images were acquired using a high-resolution transducer (MS550S). To ensure optimal image quality, fur from the abdominal region was removed using a commercial hair remover and pre-warmed ultrasound gel was applied to the skin. The B-mode was used to monitor gestational sac length, crown rump length, biparietal diameter, abdominal circumference, placental diameter, and placental thickness. Color Doppler mode was used to monitor fetal heart rate, and Power Doppler mode was used to monitor umbilical artery peak velocity. Images were saved as static images or cine loops. The imaging data sets for all mice were analyzed using Vevo 2100 built-in software.

## TUNEL assay

Apoptotic cells were detected using the FragEL DNA Fragmentation Detection Kit (Calbiochem,

Germany) according to the manufacturer's instructions. Briefly, deparaffinized placental sections were incubated with terminal deoxynucleotidyl transferase (TdT) enzyme in TdT buffer in a humidified chamber at 37°C, and tagged nucleotides were detected using fluorescein-FragEL TdT conjugates. Sections were placed under a coverslip with a mounting medium containing DAPI and examined under a fluorescence microscope (Olympus BX53, Japan).

To quantify apoptotic cells, TUNEL-positive cells were counted using ImageJ (NIH) by examining ten random fields for each placenta per experimental condition. The apoptotic index was calculated as the percentage of nuclei exhibiting TUNEL-positive staining divided by the total number of DAPI-stained nuclei in each section.

## IVIS *in vivo* imaging

To evaluate targeting by pICSA-INPs, pregnant mice at E12.5 or E15.5 were administered pICSA-INPs or SCR-INPs (5 mg/kg ICG equivalent) in tail veins. The mice were then scanned using an IVIS spectrum instrument (Perkin Elmer). Scans were taken at time intervals ranging from 10 min to 48 h. Data analysis was performed using Living Image Software (Caliper Life Sciences, CA).

## High-performance liquid chromatography analysis

MTX concentrations in fetal and placental tissues were determined by high-performance liquid chromatography (HPLC). Mice were injected intravenously with PBS, free MTX, MNPs, SCR-MNPs, or pICSA-MNPs (1 mg/kg MTX equivalent). At predetermined time points, the mice were anesthetized with 30% urethane, and following cardiac perfusion with PBS to remove unbound nanoparticles, tissues were harvested and weighed. Tissues (~200 mg) were homogenized in a volume of PBS (pH 7.4) equivalent to twice the tissue weight, 200 µL 10% perchloric acid (v/v) was added, and the mixture was vortexed for 3 min and centrifuged at 14,000×g for 20 min to pellet proteins. The supernatants were then filtered through a Millipore Swineex syringe adapter (0.45 µm), and a total volume of 20 µL was injected into the HPLC system, which consisted of an LC20A VP solvent pump, an SPD-20A UV spectrophotometric detector (Shimadzu, Kyoto, Japan), and a 250×4.6 mm (i.d.) XTerra MS C<sub>18</sub> column (5 µm particle size; Waters, MA, USA). A mixture of 40 mM potassium phosphate dibasic (pH 4.5) and acetonitrile (88:12, v/v) was used as the mobile phase, with a flow rate of 1.0 mL/min. The HPLC analysis was monitored by detecting ultraviolet absorbance at 313 nm [24].

## Study approval

Pregnant women receiving care at the Bao'an Maternal and Child Health Care Hospital of Shenzhen were enrolled in this study after providing written informed consent according to a protocol approved by the Shenzhen Institutes of Advanced Technology, Chinese Academy of Sciences Research Board. All mouse experiments were approved by the Animal Care and Use Committee of Shenzhen Institutes of Advanced Technology, Chinese Academy of Sciences.

## Statistics

All data are expressed as the mean $\pm$ SD. Univariate analyses comparing measurements and embryonic days were performed using Spearman's rank correlation (Rs). Continuous linear regression was adopted for multivariate analysis of significant parameters. All statistical tests were two-sided, and a *p* value <0.05 was considered statistically significant. Statistical analyses were performed using GraphPad Prism 6.01 (GraphPad Software Inc. USA).

## Results

### plCSA-BP specifically binds to a distinct placental-type CSA expressed on trophoblasts

To examine whether synthetic plCSA-binding peptide (plCSA-BP) could be exploited for placental targeting, biotin-plCSA-BP and biotin-SCR were incubated with mouse and human placental tissue sections and detected by histochemical techniques. Biotin-plCSA-BP efficiently bound to the trophoblast cells in the labyrinth layer, the trophoblast lining of the remodeled spiral arteries, but not to the placental chorionic plate, junctional zone, or deciduas (**Figure 1A**). Similarly, in human placenta, biotin-plCSA-BP specifically bound to the syncytiotrophoblast (**Figure 1B**), which is in line with the fact that *P.falciparum*-infected VAR2CSA-expressing erythrocytes are sequestered to the placental syncytiotrophoblast [13, 14]. Moreover, no specific binding of biotin-SCR to placental tissues was detected (**Figure 1C**).

Considering that chondroitin sulfate A (CSA) distribution is broad, with expression in several tissues [25], we also analyzed the interaction between plCSA-BP and other tissues. Staining with anti-C4S (2B6) revealed that CSA is abundant in most tissues, while none of the tissues analyzed (other than placental tissue) displayed plCSA-BP staining (**Figure 1D**). Moreover, plCSA-BP and CSA are co-localized in the mouse labyrinth and human placental syncytiotrophoblast (**Figure S1**). Thus, the data demonstrate that the plCSA-BP synthesized in this

study binds with high affinity and specificity to a placental-type CSA (plCSA) expressed exclusively on trophoblasts.

### plCSA-BP binds specifically to trophoblasts throughout gestation in the mouse

In order to test the ability of plCSA-BP to specifically bind to trophoblasts and not to other tissues throughout pregnancy, co-localization of the trophoblast marker cytokeratin 8 (CK8) and biotin-plCSA-BP was confirmed in mouse placenta at gestational stages E6.5, E8.5, E10.5, and E12.5 (**Figure 2**), and no plCSA-BP staining was detected in embryos, junctional zones, and deciduas. Along with our finding of placenta-specific plCSA-BP staining at E14.5 (**Figure 1A**), these results show that plCSA-BP specifically binds to trophoblast throughout gestation in the mouse.

### Synthesis and characterization of nanoparticles

Next, we conjugated plCSA-BP to nanoparticles. MNPs and INPs were self-assembled from MTX or ICG with PLGA, soybean lecithin, and DSPE-PEG-COOH using a single-step sonication method [11]. SCR and plCSA-BP were then conjugated to the nanoparticles by linking the amino-terminus of each peptide to carboxyl groups on the surfaces of the nanoparticles to produce SCR-MNPs/SCR-INPs and plCSA-MNPs/plCSA-INPs (**Figure 3A**).

We next determined the physical properties of these nanoparticles. The mean diameters of the MNPs, SCR-MNPs, and plCSA-MNPs were approximately 76 nm, 98 nm, and 109 nm, respectively, with good polydispersity (PDI; a measure of the heterogeneity of sizes of molecules or particles in a mixture; for a uniform sample, PDI=1.0) (**Figure 3B** and **Table 1**). Conjugation with either plCSA-BP or SCR increased the MNP sizes. Transmission electron microscopy revealed that MNPs, SCR-MNPs, and plCSA-MNPs had spherical shapes and uniform size distributions (**Figure 3C**). Zeta potentials (the nature of the electrostatic potential near the surface of a particle; if it less than -15 mV, it usually represents the onset of agglomeration, and the higher the absolute zeta potential, the more stable the particle) were -21.3 $\pm$ 2.65 mV, -24.6 $\pm$ 2.48 mV, and -27.8 $\pm$ 4.25 mV for MNPs, SCR-MNPs, and plCSA-MNPs, respectively. Hence, these nanoparticles are predicted to be highly stable. The efficiencies of plCSA-BP and SCR conjugation to MNPs were determined to be 52.3  $\pm$  4.4% and 56.1  $\pm$  3.7%, respectively (**Table 1**).

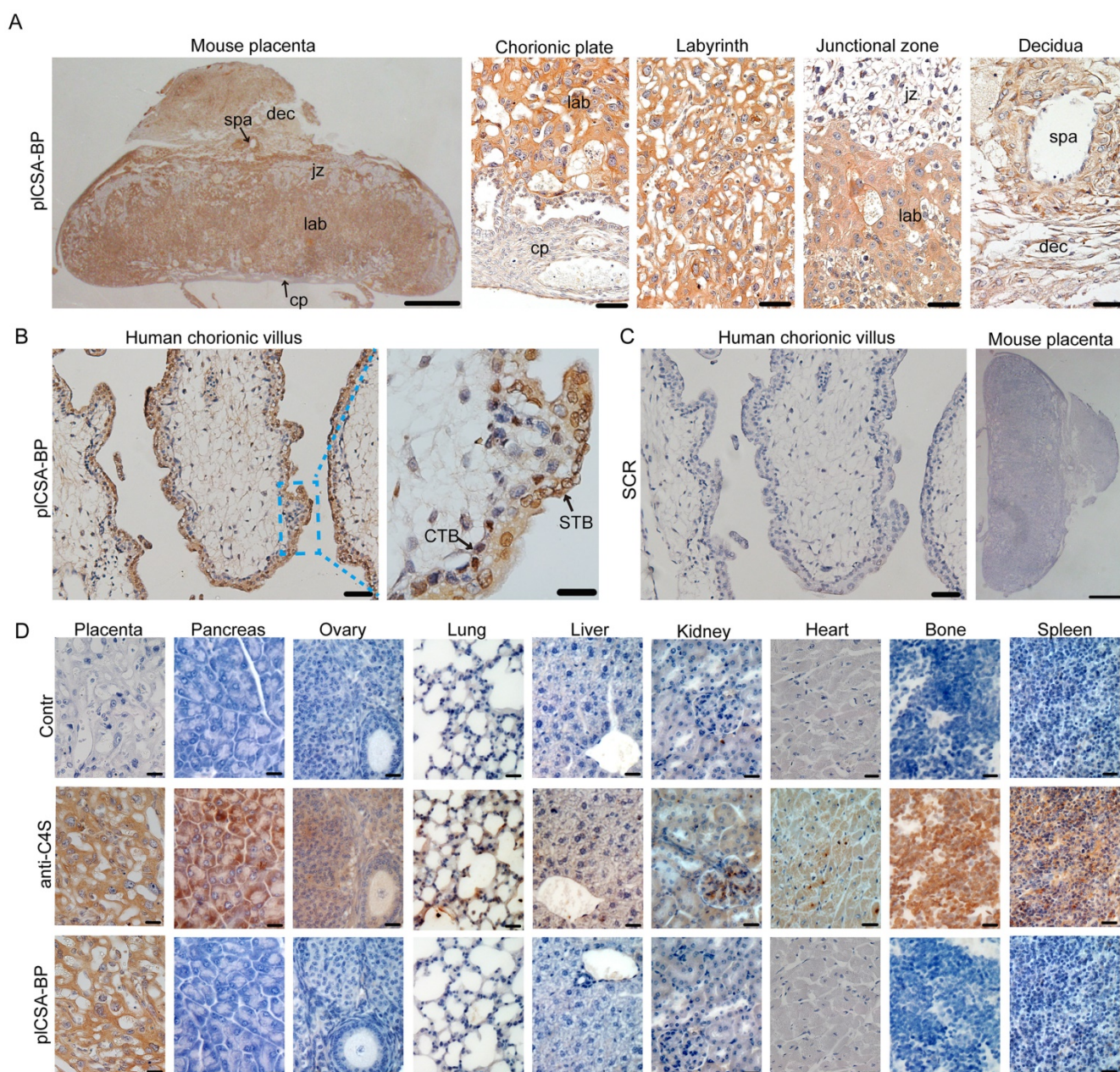


**Figure 1.** pICSA-BP specifically binds to placental tissues. **(A)** Images of full-thickness mouse placenta (left scale bar=1 mm) at E14.5 and magnified images of the chorionic plate (cp), labyrinth (lab), junctional zone (jz), decidua (dec) and spiral artery (spa) (right scale bar=50  $\mu$ m). Placenta incubated with 50 ng/mL biotin-pICSA-BP and 1:200 HRP-streptavidin. **(B)** Human placenta chorionic villus stained as in (A) (left scale bar= 50  $\mu$ m, right scale bar=20  $\mu$ m). **(C)** Representative images of indicated tissue specimens incubated with 50 ng/mL biotin-SCR and detected by HRP-streptavidin (left scale bar= 50  $\mu$ m, right scale bar=1 mm). **(D)** A selection of 9 normal mouse tissues stained for total CSA using enzymatic GAG end-processing and 1:20 anti-C4S (2B6) or for CS detected by biotin-pICSA-BP as in (A). Images representative of n=4. Scale bar=20  $\mu$ m. CTB: cytotrophoblasts; STB: syncytiotrophoblasts. See also **Figure S1**.

Drug encapsulation efficiency, drug loading efficiency, and release ability of nanoparticles are crucial parameters for determining their clinical usefulness. The drug encapsulation efficiency and drug loading efficiency of the MNPs were  $37.2 \pm 1.54\%$  and  $5.5 \pm 0.36\%$ , respectively, indicating a high drug-loading capability. The *in vitro* release profiles of the MNPs, SCR-MNPs, and pICSA-MNPs revealed

similar biphasic patterns (**Figure 3D**), characterized by a fast initial release within the first 24 h (~40% released) and a slower continuous release in the subsequent 48 h (~60%). Moreover, these results suggested that modifications with different peptides did not influence the *in vitro* release pattern of MTX from the lipid-polymer nanoparticles.

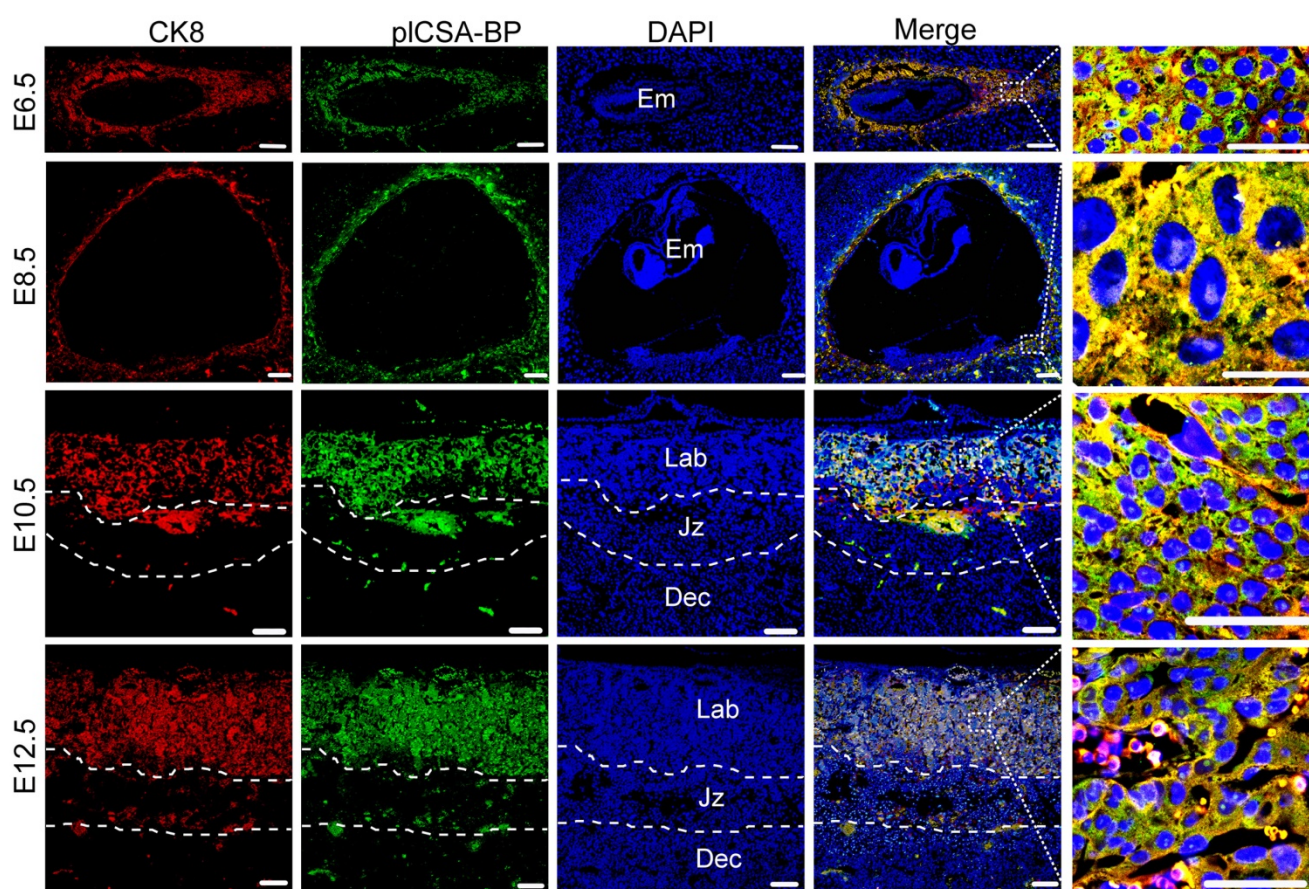


**Figure 2.** pICSA-BP specifically binds to trophoblasts during gestation in mice. Immunofluorescence staining of trophoblasts (CK8, red) and biotin-pICSA-BP (green) stained midline sections from mice at E6.5, E8.5, E10.5 and E12.5 showing that pICSA-BP is co-localized with trophoblasts in the placenta. Nuclei are counter-stained with DAPI, shown in blue. (n=4, scale bar=200  $\mu$ m (50  $\mu$ m in magnified pictures)). Dec: decidua; Em: embryo; Jz: junctional zone; Lab: labyrinth.

Next, the *in vitro* stabilities of MNPs, SCR-MNPs, and pICSA-MNPs were investigated by dispersing the nanoparticles in 10% fetal bovine serum (FBS) and examining changes in size (**Figure 3E**). The particle sizes of MNPs, SCR-MNPs, and pICSA-MNPs remained near the initial particle sizes without aggregation and precipitation over a one-month period, suggesting excellent stability for all three, which is suitable for *in vivo* experiments.

### **In vivo placenta targeting of pICSA-INPs**

To investigate the placenta-targeting ability of pICSA-BP-conjugated nanoparticles *in vivo*, we synthesized SCR- and pICSA-BP-conjugated nanoparticles loaded with infrared fluorescent ICG (SCR-INPs and pICSA-INPs). SCR-INPs and pICSA-INPs were administered to pregnant mice by intravenous injection, and the tissue distributions and localization of the nanoparticles were monitored with the IVIS live animal imaging system. ICG signal from the uterus region was observed as early as 30 min after injection, reaching a peak at 3 h, and a strong signal was maintained upto 12 h (**Figure 4A, F**). The SCR-INPs also produced strong signals in the liver region after 30 min but were at very low levels at 12 h

(**Figure 4A**). These results indicate that non-targeted nanoparticles are rapidly metabolized and eliminated by the liver after intravenous injection. Moreover, the signal from the pICSA-INPs could be detected in the uterus upto 48 h after injection based on *ex vivo* examination (**Figure 4B, G**). Notably, this signal was only found in placentas and not at all in fetuses (**Figure 4C**).

We next performed a detailed examination of placentas 48 h after a single pICSA-INP or SCR-INP injection by immunostaining for a vascular endothelial cell marker (CD31) and the trophoblast marker cytokeratin 8 (CK8) to visualize co-localization with ICG. ICG was mainly co-localized with the trophoblast, identified by CK8 staining (**Figure 4E**), with little or no staining in endothelial cells (**Figure 4D**) in the pICSA-INP group, and there was little or no ICG signal in the SCR-INP group (**Figure 4D-E, H** and **Figure S2**, showing a different serial section). These results indicate that pICSA-INPs target delivery of ICG to trophoblast. Together, these data suggest that pICSA-BP can be used as a targeting peptide for the efficient delivery of drug-loaded nanoparticles to the placenta *in vivo*.

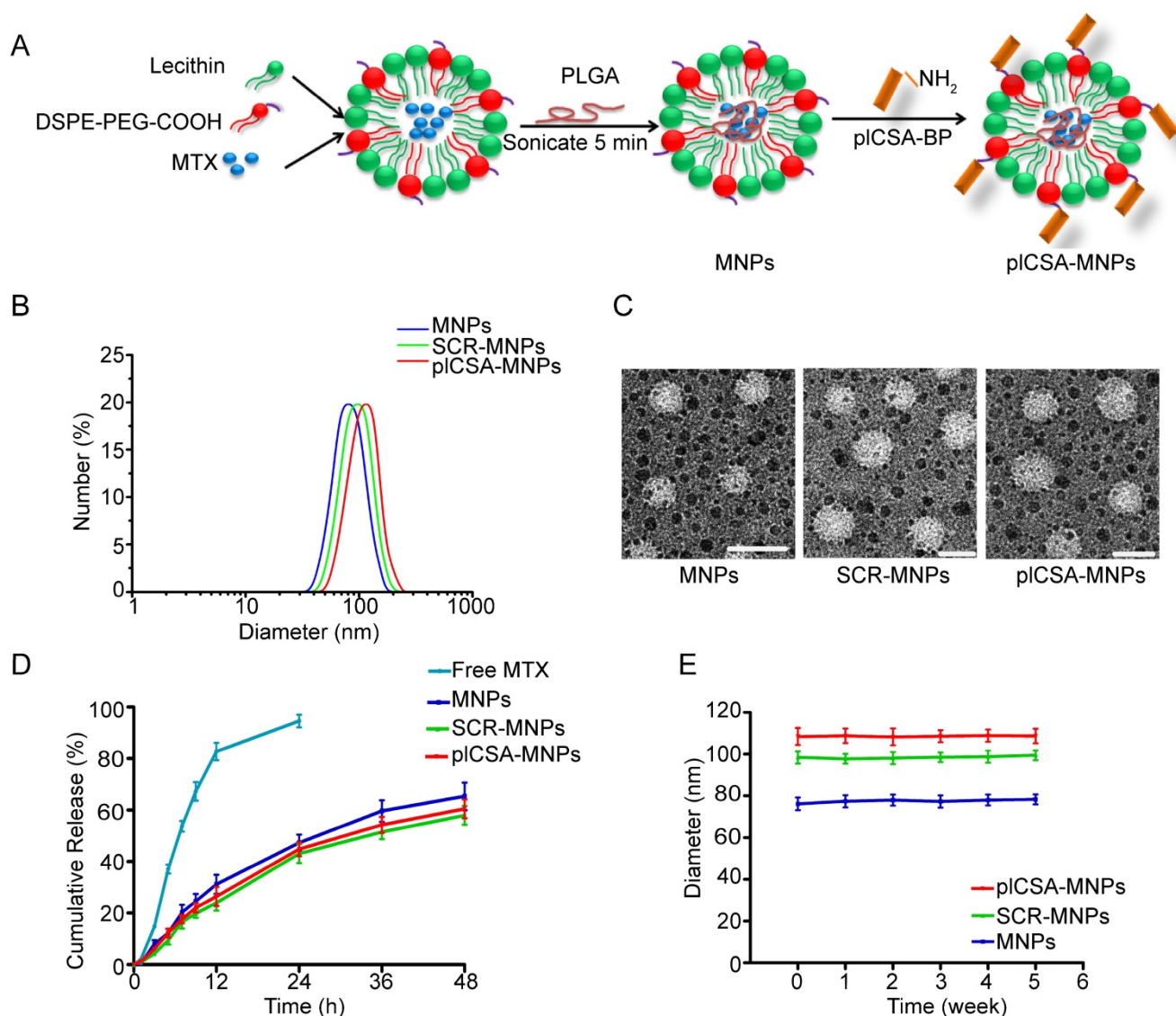


**Figure 3. Synthesis and characterization of nanoparticles.** (A) Schematic illustration of the single-step sonication process used to synthesize MNPs and the EDC/NHS reaction scheme used for conjugation with the pICSA-BP. (B) Diameter distributions of different nanoparticles measured by dynamic light scattering (DLS). (C) Representative TEM images of MNPs, SCR-MNPs, and pICSA-MNPs. Scale bars=100 nm. (D) Time course of MTX release from MNPs, SCR-MNPs, and pICSA-MNPs in PBS (pH7.4) at 37°C. (E) Nanoparticle stability in serum (10% FBS) was evaluated by examining size changes. Data are shown as the mean±SD (n=4).

**Table I. Characterization of the nanoparticles**

	Diameter (nm)	Zeta potential (mV)	Polydispersity	EE of MTX (%)	LE of MTX (%)	Conjugation efficiency (%)
MNPs	76.2±5.3	-21.3±2.65	0.102±0.023	37.2±1.54	5.5±0.36	-
SCR-MNPs	98.4±4.6**	-24.6±2.48	0.124±0.045	-	-	56.1±3.7
pICSA-MNPs	108.5±7.6**	-27.8±4.25	0.108±0.073	-	-	52.3±4.4

\*\*p<0.01 compared with MNPs (n=3).

EE: drug encapsulation efficiency.

LE: drug loading efficiency.

### Quantitative analysis of embryonic growth after the administration of pICSA-MNPs

MTX, a drug used to treat ectopic pregnancy and choriocarcinoma, was selected to test the efficiency and effectiveness of pICSA-BP-conjugated nanoparticles as drug delivery vehicles to the trophoblast in the placenta. The effects of pICSA-MNPs were

compared to those of free MTX, MNPs, and SCR-MNPs on placental and fetal development in pregnant mice from early to later pregnancy (E6.5-E14.5) and on pregnancy outcomes based on high-frequency ultrasound (HFUS). Treatment with pICSA-MNPs significantly reduced gestational sac length, crown rump length, biparietal diameter, abdominal circumference, placental diameter, and

placental thickness (Figure 5A-F and Movies S1-2). Fetal heart rate and umbilical artery blood flow velocities also significantly decreased compared to those of the control groups (Figure 5G-H). The growth of both fetuses and placentas was slightly inhibited by free MTX, but the difference did not reach significance (Figure 5A-H). Pregnant mice treated with MNPs or SCR-MNPs showed impaired fetal development, and the survival rate of these two groups was approximately 83%. Remarkably, the pICSA-MNPs exerted a strong cytotoxic effect on both placental and fetal development, which decreased fetal survival rates to less than 10% at E14.5 (Figure 5I).

### HFUS evaluation of embryo morphology after the administration of pICSA-MNPs

Whole-embryo images at each stage from E6.5 to E14.5 were acquired by high-frequency ultrasound (HFUS) and used to assess physiological fetal and placental growth. On day E8.5, the S-shaped embryo starts to turn around its own axis, the allantois, which later gives rise to the umbilical vessels; this movement was visible in the PBS and free MTX groups (Figure 6A-B). Although the embryos were visible, compared to those in the PBS group, the embryonic cavities were smaller (Figure 6C-F) in the mice treated with MNPs, SCR-MNPs, and pICSA-MNPs.

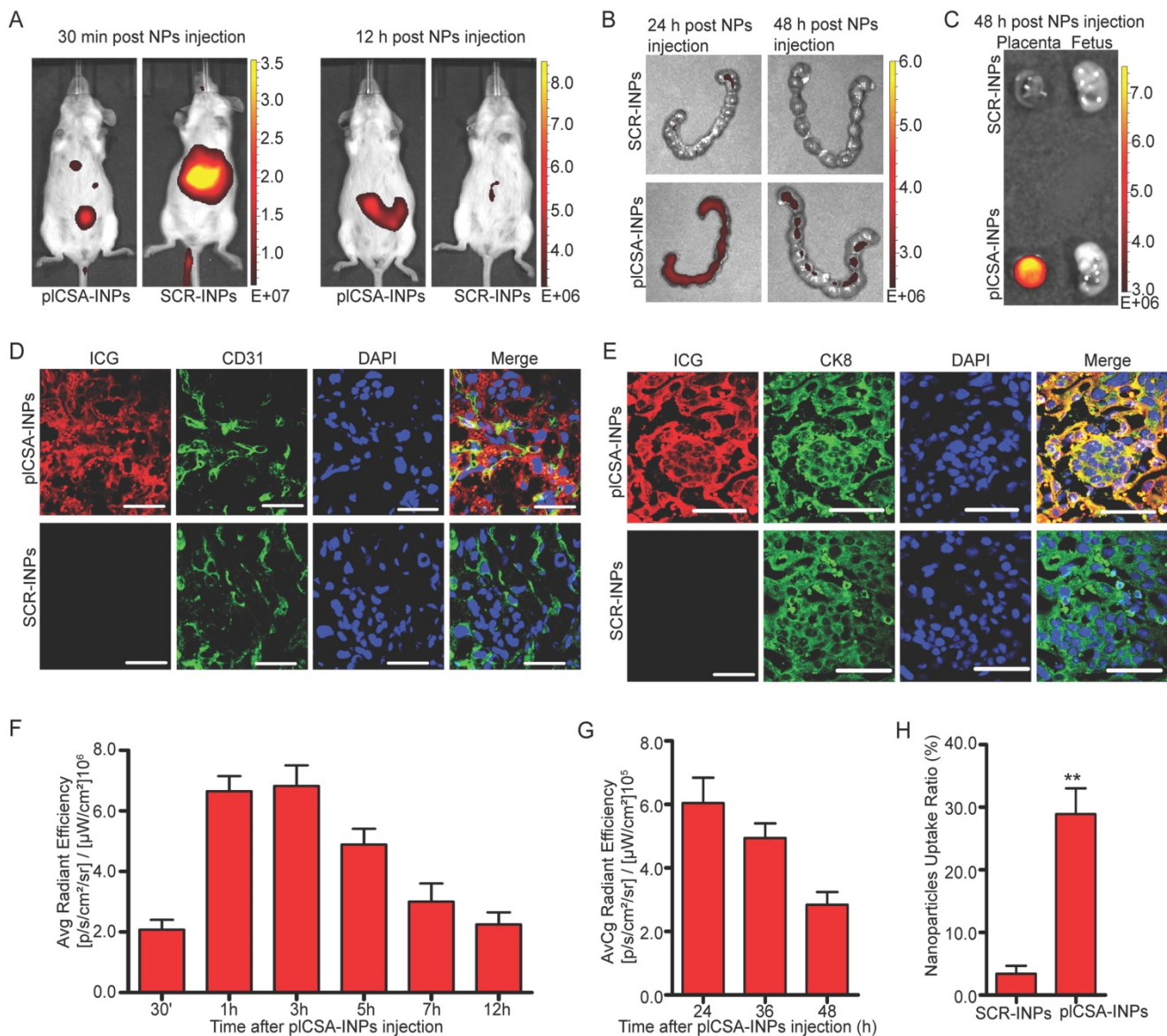


**Figure 4.** *In vivo* placenta targeting by using pICSA-INPs. (A) Pregnant mice at E12.5 (n=5 each) were injected with SCR-INPs or pICSA-INPs (ICG, equivalent 5 mg/kg) via the tail vein and imaged with an IVIS spectrum optical imaging system. (B) *Ex vivo* detection of the ICG signal in uteri by IVIS. (C) Forty-eight hours after intravenous injection of SCR-INPs or pICSA-INPs at E15.5 (n=5 each). (D-E) Representative immunofluorescence images of placental middle sections. SCR-INPs or pICSA-INPs (ICG, red, equivalent 5mg/kg) were injected into the tail vein of pregnant mice. After 48 h, mice were subjected to cardiac perfusion to remove unbound nanoparticles. Placentas were collected, and serial sections were immunostained for CD31 (green) or CK8 (green) and examined by confocal microscopy. DAPI, blue. Scale bar=50  $\mu\text{m}$ . Images representative of n=6. (F-G) Quantification of the IVIS signal from pregnant mice (E12.5) after injection with pICSA-INPs at different time points from 30 min to 48 h. (H) Quantitative analysis of cell-associated nanoparticles as in (E); ICG-positive cells were counted using ImageJ in ten random fields per experimental condition. Values are expressed as the mean  $\pm$ SD (n=6). \*\*p< 0.01. See also Figure S2.

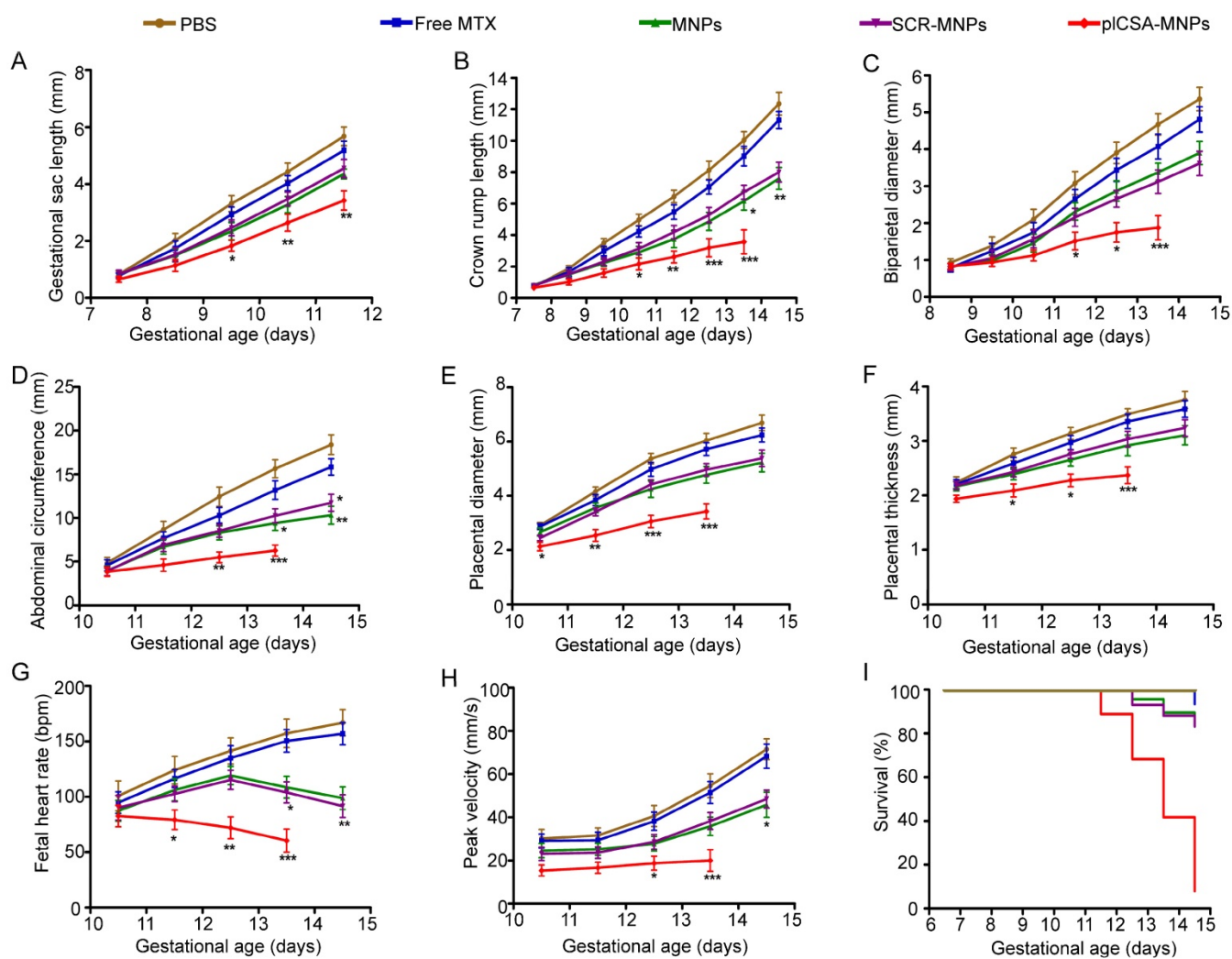


**Figure 5. Embryonic growth quantified using ultrasound parameters after various treatments.** (A) Gestational sac length (n=10-30 embryos/day), (B) crown rump length (n=30-51 embryos/day), (C) biparietal diameter (n=30-51 embryos/day), (D) abdominal circumference (n=30-51 embryos/day), (E) placental diameter (30-51 embryos/day), (F) placental thickness (30-51 embryos/day), (G) fetal heart rate (n=20-33 embryos/day) and (H) umbilical artery peak velocity (n=12-36 embryos/day) measured non-invasively by ultrasound *in vivo*. (I) Fetal survival curves for different treatments (n=45-55 embryo). At pregnancy day 6.5, mice received intravenous injections of different nanoparticles; treatment was administered every 2 days. Values are expressed as the mean  $\pm$ SD. \* $p < 0.05$ , \*\* $p < 0.01$ , \*\*\* $p < 0.001$  vs. the free MTX group.

On day E10.5, the embryos were considerably larger in size, and the hearts could be clearly distinguished by ultrasound. Although the placentas exhibited an echogenicity similar to that of the decidua basalis, they could be differentiated by their pulsating blood vessels and layers of higher echogenicity between the embryonic trophoblast and maternal decidua in the PBS and free MTX groups (Figure 6G-H). The fetuses had shorter crown rump lengths in the MNP and SCR-MNP groups (Figure 6I-J), while the placenta showed calcification in the pICSA-MNP group, as described by Akirav *et al.* [26]. The concretions most likely originated from dystrophic calcification processes in dysfunctional cells, where active calcium transport is impaired. Growth-retarded embryos also exhibited bradycardia (Figure 6K-L and Movie S3).

On day E12.5, the umbilical cord that links the fetus to the placental chorionic plate was present in

the PBS control group (Figure 6M). In contrast, the fetuses showed growth retardation in the free MTX group (Figure 6N) and were smaller in the MNP and SCR-MNP groups compared to the PBS group (Figure 6O-P). However, in the pICSA-MNP group, the fetuses showed pericardial edema, and placentas were smaller, with higher echogenicity, and approximately 50% of the fetuses were dead (Figures 6Q-R).

On day E14.5, the fetuses were considerably larger in the PBS group (Figure 6S). In contrast, in the free MTX group, the fetuses were smaller (Figure 6T). The placentas showed calcification, and approximately 30% of the fetuses were dead in the MNP and SCR-MNP groups; no significant difference ( $P > 0.05$ ) was found between these two groups (Figure 6U-V and Figure S3). However, in the pICSA-MNP group, more than 90% of the fetuses were dead and resorbed (Figure 6W-X).

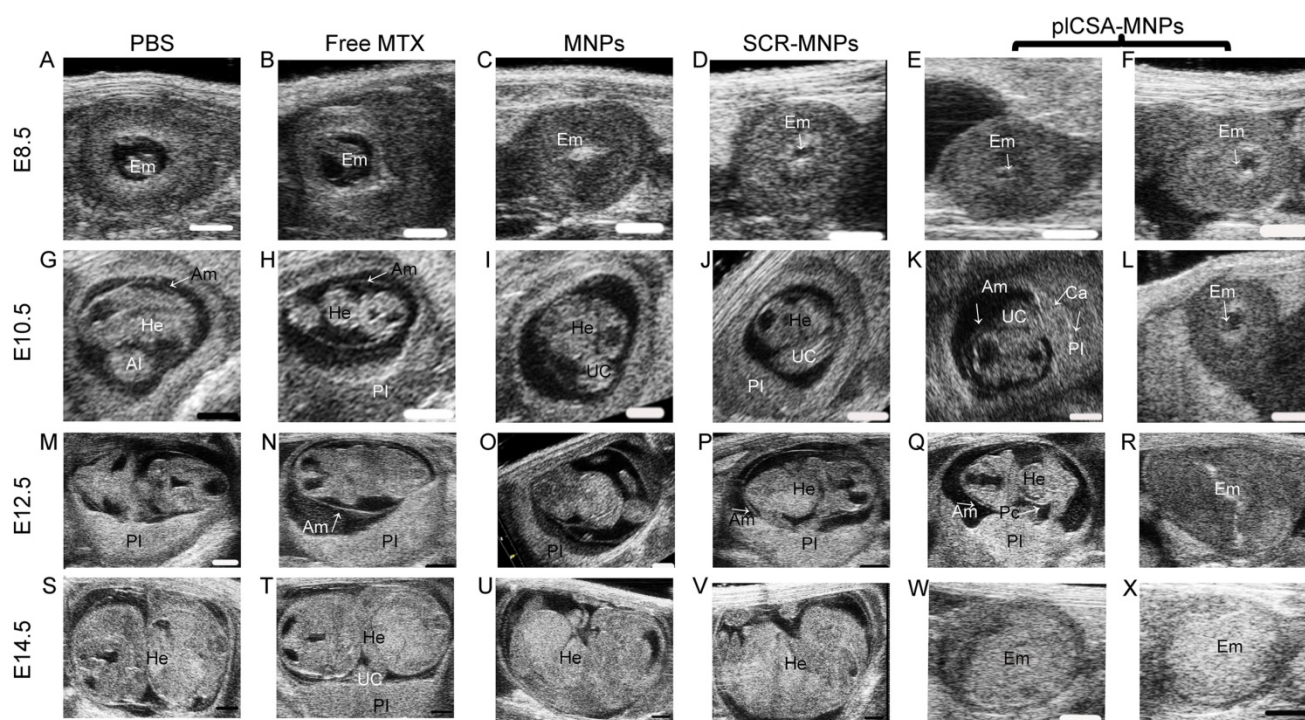


**Figure 6.** HFUS evaluation of embryo morphology after the administration of free MTX and different nanoparticles. At E6.5, mice ( $n=6$  each) received intravenous injections of free MTX or MTX-containing different nanoparticles (1 mg/kg MTX equivalent); treatment was administered every 2 days. Embryonic growth was measured using a Vevo 2100 ultrasound imaging system. (A-B) The embryonic cavity and the embryo (Em) are visible. (C-F) Note the small embryonic cavity (arrows). (G-J) The embryonic heart (He) could be distinguished by ultrasound. (K) The placenta displays hypercholesterolemic calcification deposits (Ca, arrows) at the fetal-maternal boundary. (L) A resorption site with a small embryonic cavity (arrow). (M-P) An embryo enlarged in size. The placenta (PI) could be differentiated by its pulsating blood vessels. (Q) An embryo exhibiting a reduced heart rate. Pericardial (Pc) effusion is evident. The placenta has a high echodensity spot and smaller size. (R) A dead embryo. (S-V) Progressive ossification is observed in the fetus. (W-X) Embryos with high echodensity spots are resorbed. Al: allantois; Am: amnion; UC: umbilical connection. Scale bars=1 mm. See also Figure S3.

### pICSA-MNPs interfere with pregnancy outcome by targeting the placenta

Next, we measured the cross-sectional areas of blood sinusoids in the placental labyrinthine region using computerized morphometry, which showed that the average blood sinusoid areas decreased markedly in the placentas of mice treated with pICSA-MNPs beginning on E10.5, and that the labyrinthine region was nearly gone at E14.5 (Figure 7A-B). Interestingly, the average blood sinusoid areas in the MNP and SCR-MNP groups were also substantially decreased at E14.5, indicating that nanoparticles might significantly improve the delivery of drug to the placenta via the enhanced permeability and retention (EPR) effect [27, 28].

To determine whether pICSA-MNPs can cross the placenta and reach the fetus, leading to serious fetal side effects, we measured MTX levels in placentas and fetuses by HPLC. Free MTX and MTX-containing nanoparticles were administered intravenously to pregnant mice. 24 h after injection, MTX was not detected in the placentas from the free MTX group, while it was detected at minimal levels in the MNP and SCR-MNP groups and at the highest

levels in the pICSA-MNP group (Figure 7C). Furthermore, it was also detected in the fetuses, although at lower levels than in the placentas, in the MNP and SCR-MNP groups. This suggested that lipid-polymer nanoparticles slightly limit transfer of MTX across the placenta. In contrast, the pICSA-MNPs had efficiently accumulated in placentas after 24 h, and MTX was detectable in placentas 48 h after injection. Notably, MTX was not detectable in the fetuses at either time point in the pICSA-MNP group (Figures 7C and Figure S4).

To confirm that pICSA-NPs delivered MTX specifically to placental trophoblasts, apoptosis was analyzed by TUNEL assay in placenta sections. After free MTX treatment, there was minimal apoptosis. As expected, MNPs and SCR-MNPs increased the levels of apoptosis in placental tissue. Notably, pICSA-MNPs vigorously increased apoptotic cell numbers. Specifically, TUNEL-positive cells were found mainly in the placental labyrinthine trophoblast (Figure 8A-B and Figure S5). Together, these data provide compelling evidence that pICSA-MNPs interfere with pregnancy outcomes by effectively targeting the placental trophoblast.

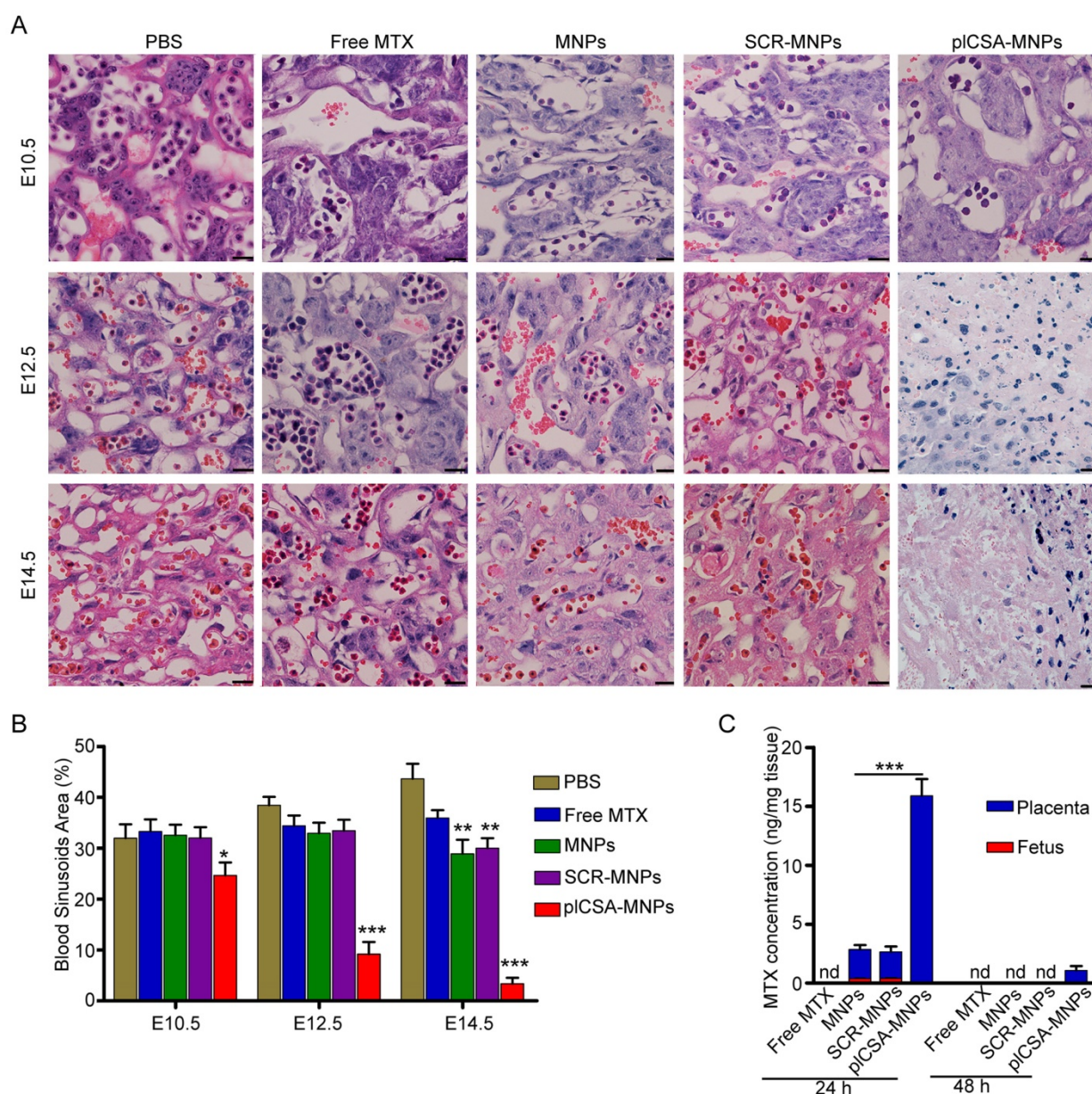


**Figure 7. Methotrexate delivered by pICSA-MNPs significantly reduces placental vascular density.** Pregnant mice ( $n=6$  for each group) received intravenous injections of different nanoparticles on E6.5. (A) Histological cross sections of the labyrinth layers from placentas ( $n=10-14$  each) of different groups stained with H&E. (B) The vascular areas in the labyrinthine regions were estimated from at least 3 non-consecutive sections from each placenta using ImageJ. Blood sinusoid cross-sectional areas were calculated as the ratio between the numbers of pixels within the area defined using the threshold function and the overall number of pixels in the image. Scale bar= $20\ \mu\text{m}$ . All data are expressed as the mean $\pm$ SD. \*\*\* $p < 0.001$  vs. PBS group. (C) HPLC measurement of MTX concentrations in placentas ( $n=15$  for each group) and fetuses ( $n=15$  for each group) 24 h and 48 h after a single injection of free MTX or MTX-containing different nanoparticles (1 mg/kg MTX equivalent) in pregnant mice ( $n=5$  for each group) at gestational stage E13.5. Values are expressed as the mean $\pm$ SD. \*\*\* $p < 0.001$  vs. the MNPs group. nd: not detected. See also Figure S4.

### pICSA-MNPs exhibit minimal liver and kidney toxicity

The toxicities of each experimental treatment in maternal liver and kidney were evaluated by histological examination of tissue sections (Figure 9). Liver sections from the PBS group revealed normal liver structure with dilated blood sinusoids. In the free MTX group, liver sections revealed necrosis of the hepatocyte inflammatory cells around the central vein, dilated blood sinusoids, and activated Kupffer cells. In addition, distortions in cell arrangement

around the central vein, pyknotic and apoptotic nuclei, and dilation of most sinusoids were observed. The liver sections in the MNP and SCR-MNP groups showed fewer abnormalities, with less hepatocyte necrosis, and fewer pyknotic nuclei, dilated blood sinusoids, and activated Kupffer cells compared to that in the free MTX group. However, liver sections from the pICSA-MNP group displayed a similar architecture similar to that in the PBS group, with intact hepatic cords, few inflammatory cells around the central vein, less hepatocyte necrosis and fewer activated Kupffer cells.

Examination of kidney sections revealed changes similar to those found in the liver sections from the different treatment groups. The kidney sections from the PBS group showed normal architecture, whereas vacuolation and pyknotic nuclei in some tubules and glomerular atrophy and dilated urinary spaces were observed in the free MTX group. In the MNP and SCR-MNP treatment groups, kidney sections showed

moderate vacuolation and pyknotic nuclei in the renal epithelia. In contrast, the kidney sections from the pICSA-MNP group showed normal tissue architecture. Collectively, these results indicate that pICSA-NPs can facilitate delivery of MTX to the placenta *in vivo* with no detrimental effects to other tissues.

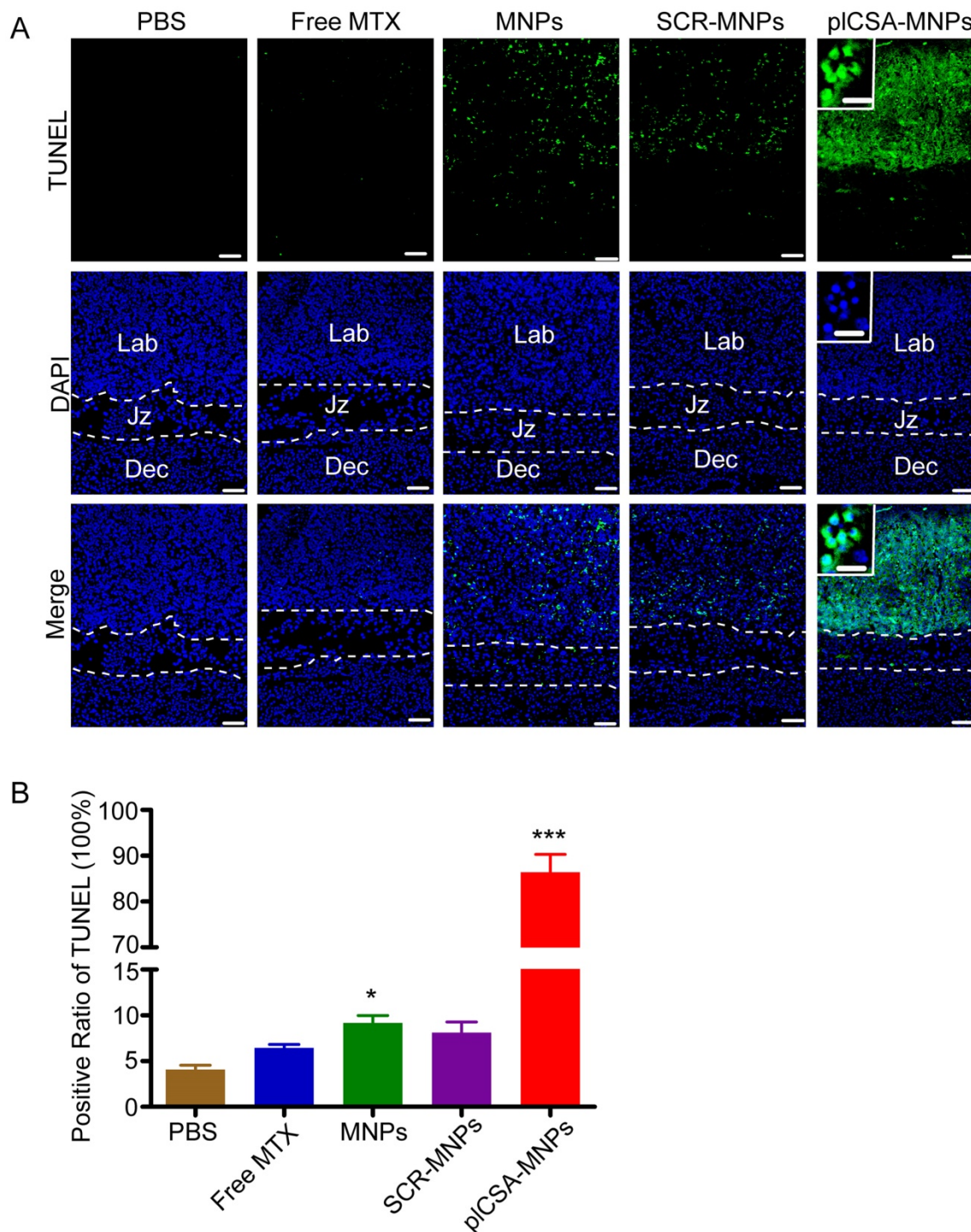


**Figure 8. Apoptosis is induced by pICSA-MNPs in the placenta, confirmed by TUNEL assay. (A)** Middle sections viewed by fluorescence microscopy. TUNEL-positive cells are stained in green, whereas blue indicates DAPI-stained nuclei. **(B)** The percentages of TUNEL-positive cells from different treatment groups. Dec, decidua; Jz, junctional zone; Lab, labyrinth. Scale bar=100 μm and white boxes represent magnifications of the indicated areas (scale bar=20 μm). Data are presented as mean ±SD (n=6). \*p< 0.05, \*\*\*p< 0.001 vs. the PBS group. See also **Figure S5**.

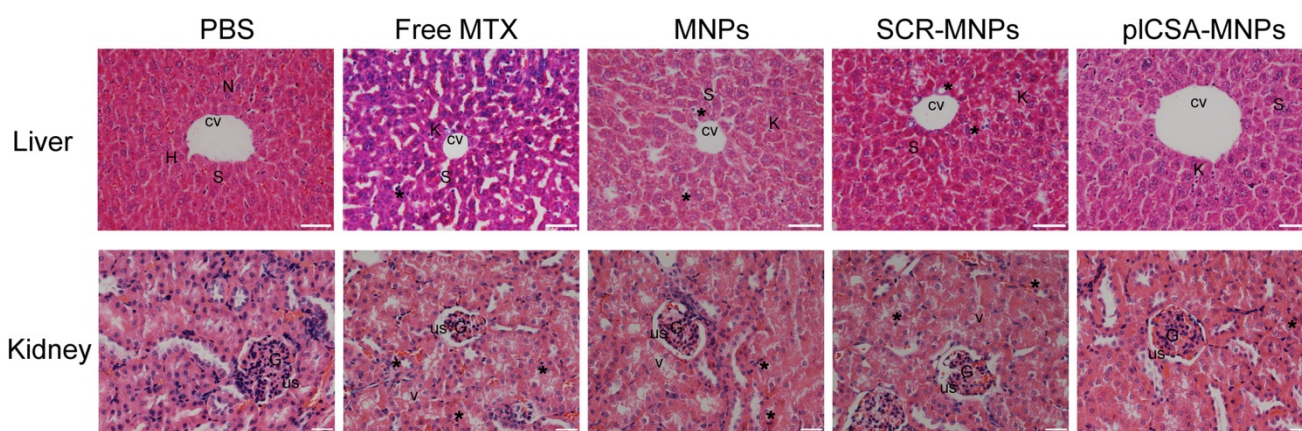


**Figure 9. Free MTX induces renal and hepatic toxicity but pICSA-MNPs do not.** The livers from the PBS group had normal histology with the central vein (CV) and hepatic cords of hepatocytes (H) having prominent nuclei (N) separated by blood sinusoids (S). The free MTX group exhibited necrosis of hepatocytes (star), the most dilated blood sinusoids (S) and the highest rate of Kupffer cell activation (K). In addition, liver images from the free MTX group reveal distortion in the cell arrangement around the central vein. Livers from the MNP and SCR-MNP groups had pyknotic nuclei (star) and like the free MTX group had dilated blood sinusoids (S). These images demonstrate moderate improvement with little necrosis of hepatocytes, dilation of blood sinusoids, or activation of Kupffer cells. Mouse livers treated with pICSA-MNPs displayed normal hepatic cells with few Kupffer cells (scale bar=50  $\mu$ m). Sections of normal kidney tissue from the PBS group verify normal architecture of glomeruli (G), urinary spaces (US), and renal tubules. In the free MTX group, the kidneys displayed vacuolation and pyknotic nuclei (star) in some tubules, glomerular atrophy and dilated urinary spaces. Kidneys from the MNP and SCR-MNP groups exhibited moderate vacuolation and pyknotic nuclei in renal epithelia, while kidneys from the pICSA-MNP group appeared nearly normal. Images representative of n=5. Scale bar= 20  $\mu$ m

## Discussion

No highly effective therapeutic agent is currently licensed to treat placental insufficiency and alleviate the resulting maternal and fetal complications. The risk of serious side effects in the fetus or mother is a major barrier to the development of medications in obstetrics. Inspired by the new insight that *P. falciparum*-infected erythrocytes bind to a distinct chondroitin sulfate (CSA) exclusively expressed in the intervillous spaces of human placentas through VAR2CSA protein [13, 14], here, we describe a novel nanoparticle drug delivery system that specifically targets trophoblasts and may be a highly effective and safe therapeutic approach to treat placenta-mediated pregnancy complications.

In this communication, we demonstrate that pICSA-BP, derived from VAR2CSA, specifically binds to human placental syncytiotrophoblasts and mouse trophoblasts throughout gestation. Furthermore, we show that nanoparticles conjugated to pICSA-BP efficiently bind to the murine placental labyrinth trophoblast cells *in vivo* and *ex vivo*, and nanoparticles decorated with pICSA-BP selectively deliver MTX to mouse placenta, producing highly specific effects not produced by untargeted MTX. Non-invasive and real-time high-frequency ultrasound imaging demonstrated that pICSA-MNPs significantly inhibited embryonic growth and increased fetal loss, unlike untargeted MTX, which had only minor effects on blood sinusoid volume. The effectiveness of pICSA-MNPs targeted to placental labyrinthine trophoblasts was evident by the marked increase in numbers of apoptotic trophoblast cells and the

decreased blood sinusoid volume in the placental labyrinthine region. More importantly, pICSA-MNPs had no adverse effects on maternal tissues and did not detectably cross the placenta from mother to fetus, did not accumulate in fetal tissues, and did not cause any apparent fetal toxicity. Together, these findings demonstrate the utility of pICSA-BP-decorated nanoparticles as a novel carrier system that can specifically accomplish the targeted delivery of drugs to the placenta.

The concepts of nanomedicine have been applied clinically for more than two decades in the fields of oncology and infectious diseases [29-31], but their application to pregnancy disorders is in its infancy. Fortunately, from an obstetrical perspective, the placental transfer of nanoparticles has been evaluated using a number of experimental models. Muothen *et al.* [32] reviewed past reports and showed that particle size, surface modifications and shape determine whether nanoparticles can cross the placenta barrier. These small and potentially toxic nanomaterials include quantum dots, polymeric nanoparticles, and those based on silica, gold, polystyrene, titanium, iron oxide, and silver, which readily cross the placental barrier and are detected within fetal circulation. Liposomes, phospholipid-based nanoparticles [7], are biodegradable and non-toxic and have been approved by the United States Food and Drug Administration. They are currently being used in clinical settings to enhance drug delivery to tumors and reduce the adverse effects of various drugs [30, 33, 34]. Recently, liposomes as a nanoparticle vehicle were investigated in pregnancy and were revealed to lack transplacental uptake; they did not cross the placental barrier to the

fetus in rodent and *ex vivo* models [8, 10, 35-37]. However, despite the placenta's unrestricted exposure to drugs in the maternal blood stream, only a relatively small fraction of maternally administered non-targeted nanoparticles have been found to be taken up by the placenta.

In recent years, several research reports have focused on targeting nanoparticles to uteroplacental tissues for the therapy of pregnancy-related complications. In the first of these, Kaitu'u-Lino *et al.* developed a nanocell for the targeted delivery of doxorubicin into placental tissues to treat ectopic pregnancies and trophoblastic tumors via surface decoration with antibodies to target the epidermal growth factor receptor (EGFR). In normal tissues, EGFR levels are low, with the exception of placental trophoblasts, in which the levels are very high [38]. In another novel study, King *et al.* showed that nanocarriers coated with the tumor-homing peptide CGKRK and iRGD efficiently deliver payloads to the mouse placenta and that these peptides bind selectively to the endothelium of established uterine spiral arteries and trophoblasts lining remodeled segments [39]. Additionally, the placenta-homing peptide CCGKRK-micro RNA inhibitor conjugates, namely, peptide nucleic acid (PNA) conjugates, have been successfully exploited for the targeted delivery of micro RNAs to the placenta [40]. Cureton *et al.* used the same phage screening approach that identified pLCSA-BP to identify other novel placenta-targeted peptides that selectively bind to the endothelium of the uterine spiral arteries and the placental labyrinth *in vivo* [41]. When the vasculature-targeting peptides were conjugated to liposomes, these liposomes selectively delivered payloads to the uteroplacental vasculature. Furthermore, as the levels of oxytocin receptor (OTR) are high in the pregnant uterus [42] and low on various tissues, including the brain and mammary tissue [43], liposomes conjugated to antibodies to the OTR have been created for the targeted delivery of payloads to the pregnant uterus [44, 45]. Targeted nanomedicines represent a new frontier in obstetrics, and the clinical need for new approaches to deliver drugs in pregnancy is substantial [46]. The pLCSA-BP-guided nano-carrier described in this study is complementary to the current uteroplacental targeting delivery methods, as it targets the placental trophoblast throughout gestation, which is lacking in current applications.

VAR2CSA-expressing parasites only adhere to the placenta; they do not bind to CSA expressed elsewhere in the body [14, 47, 48]. Placental CSA (pLCSA) may therefore be a distinct CS subtype expressed exclusively in the placenta. This notion was supported by our experiments, in which we

demonstrated that synthetic pLCSA-BP specifically and efficiently binds to a distinct pLCSA expressed exclusively in the placental trophoblast and not in other tissues *in vitro* and *in vivo*. The excellent characteristic of pLCSA-BP selectively targeted to the placenta minimized the risk of off-target side effects of payloads. Minimizing fetal exposure and other maternal tissue/organ exposure to a drug is an important aspect of developing safer drug for use in pregnancy. The pLCSA-BP-coated nanoparticles will make it possible to deliver some drugs that could improve placental vascular function but have side effects for the mother, for example, sildenafil citrate in treatment of fetal growth restriction [49, 50]. In the current study, we have shown that pLCSA-BP-conjugated MNPs did not cross the placenta to accumulate in the fetus. More importantly, non-targeted lipid-polymer nanoparticles did cross the placental barrier. The nanoparticles changing from crossing the placenta to not crossing the placenta indicate that pLCSA-BP efficiently binds to the placental tissue, minimizing the transport of associated nanoparticles across the placental barrier. Additionally, pLCSA-NPs loaded with MTX gave no evidence of adverse effects on maternal tissues.

For targeted nanoparticles to be adopted and accepted in the clinic, further research and development will be required, including optimization of nanoparticles formulations, candidate payloads, drug encapsulation protocols, and dosing regimens to maximize drug delivery. In addition, toxicity testing in appropriate animal models and a comparison of how effectively they treat pregnancy complications against current therapies are necessary.

In summary, our technology facilitates the targeted delivery of drugs to the placenta and provides a novel platform for the development of placenta-specific therapeutics. We believe that the pLCSA-BP is a highly effective tool that can be used to deliver large amounts of therapeutic drugs specifically to the placenta.

## Abbreviations

AC: abdominal circumference; BPD: biparietal diameter; CK8: cytokeratin 8; cp: placental chorionic plate; CRL: crown-rump-length; dec: decidua; EE: drug encapsulation efficiency; Em: embryo; EPR: enhanced permeability and retention; GSL: gestational sac length; HFUS: high-frequency ultrasound; HPLC: high-performance liquid chromatography; HR: heart rate; ICG: indocyanine green; IEs: infected erythrocytes; jz: junctional zone; lab: labyrinth; LE: drug loading efficiency; MTX: methotrexate; PD: placental diameter; pLCSA: placental-type chondroitin sulfate A; PT: placental thickness; spa: spiral arteries;

TEM: transmission electron microscopy; TUNEL: Terminal deoxynucleotidyl transferase dUTP nick-end labeling; UA: umbilical artery.

## Acknowledgments

The authors would like to thank Fei Yan at the Paul C. Lauterbur Research Center for Biomedical Imaging of SIAT for the provision of ultrasound machines. We also thank Matt Petitt, PhD, for his comments and editorial assistance in preparation of the manuscript. This work was supported by grants from the National Key Research and Development Program of China (2016YFC1000402), the National Natural Sciences Foundation (81571445 and 81771617) and Natural Science Foundation of Guangdong Province (2016A030313178) to X.F.; Shenzhen Basic Research Fund (JCYJ20150521094519488) to X.F. and (JCYJ20170413165233512) to J.Z. and X.F.; Public Welfare Project of Guangdong Province (2017A020211033) to J.Z., and US National Institute of Child Health and Human Development (HD088549-01) to N.N.; National Natural Science Foundation of China (31571013 and 81501580), Key International S&T Cooperation Project (2015DFH50230) to L.C.

## Supplementary Material

Movie S1. <http://www.thno.org/v08p2765s1.mkv>

Movie S2. <http://www.thno.org/v08p2765s2.mkv>

Movie S3. <http://www.thno.org/v08p2765s3.mkv>

Supplementary Figures.

<http://www.thno.org/v08p2765s4.pdf>

## Author contributions

X.F., B.Z., L.T., B.A., N.N., J.Z., and L.C. conceived the study. B.Z., X.F. and L.T. designed research studies. B.Z., L.T., Y.Y., B.W., J.H., J.C., Z.C., and M.L. conducted experiments. B.Z., X.F., L.T., T.X., and Q.Y. analyzed data. B.Z., B.A., N.N. and XF wrote the manuscript. All authors reviewed and proofed the manuscript.

## Competing Interests

X.F., B.Z., and J.Z. are inventors on patent application PCT/CN2017/108646 submitted by SIAT that covers a placenta-specific drug delivery method and its application. All other authors declare that they have no competing interests.

## References

1. Stillbirth Collaborative Research Network Writing Group. Causes of death among stillbirths. *Jama*. 2011; 306: 2459-68.
2. Berg CJ, Atrash HK, Koonin LM, Tucker M. Pregnancy-related mortality in the United States, 1987-1990. *Obstet Gynecol*. 1996; 88: 161-7.
3. Cantwell R, Clutton-Brock T, Cooper G, Dawson A, Drife J, Garrod D, et al. Saving Mothers' Lives: Reviewing maternal deaths to make motherhood safer: 2006-2008. The Eighth Report of the Confidential Enquiries into Maternal Deaths in the United Kingdom. *BJOG*. 2011; 118 (Suppl 1): 1-203.

4. Fisk NM, Atun R. Market failure and the poverty of new drugs in maternal health. *PLoS Med*. 2008; 5: e22.
5. Fisk NM, McKee M, Atun R. Relative and absolute addressability of global disease burden in maternal and perinatal health by investment in R&D. *Trop Med Int Health*. 2011; 16: 662-8.
6. Syme MR, Paxton JW, Keelan JA. Drug transfer and metabolism by the human placenta. *Clin Pharmacokinet*. 2004; 43: 487-514.
7. Riehemann K, Schneider SW, Luger TA, Godin B, Ferrari M, Fuchs H. Nanomedicine—challenge and perspectives. *Angew Chem Int Ed Engl*. 2009; 48: 872-97.
8. Bajoria R, Sooranna S, Chatterjee R. Effect of lipid composition of cationic SUV liposomes on materno-fetal transfer of warfarin across the perfused human term placenta. *Placenta*. 2013; 34: 1216-22.
9. Refuerzo JS, Godin B, Bishop K, Srinivasan S, Shah SK, Amra S, et al. Size of the nanovectors determines the transplacental passage in pregnancy: study in rats. *Am J Obstet Gynecol*. 2011; 204: 546. e5-9.
10. Refuerzo JS, Alexander JF, Leonard F, Leon M, Longo M, Godin B. Liposomes: a nanoscale drug carrying system to prevent indomethacin passage to the fetus in a pregnant mouse model. *Am J Obstet Gynecol*. 2015; 212: 508. e1-7.
11. Zheng M, Yue C, Ma Y, Gong P, Zhao P, Zheng C, et al. Single-step assembly of DOX/ICG loaded lipid-polymer nanoparticles for highly effective chemo-photothermal combination therapy. *ACS nano*. 2013; 7: 2056-67.
12. Zhao P, Zheng M, Yue C, Luo Z, Gong P, Gao G, et al. Improving drug accumulation and photothermal efficacy in tumor depending on size of ICG loaded lipid-polymer nanoparticles. *Biomaterials*. 2014; 35: 6037-46.
13. Salanti A, Staalsoe T, Lavstsen T, Jensen AT, Sowa M, Arnot DE, et al. Selective upregulation of a single distinctly structured var gene in chondroitin sulphate A-adhering *Plasmodium falciparum* involved in pregnancy-associated malaria. *Mol Microbiol*. 2003; 49: 179-91.
14. Salanti A, Dahlbäck M, Turner L, Nielsen MA, Barfod L, Magistrado P, et al. Evidence for the involvement of VAR2CSA in pregnancy-associated malaria. *J Exp Med*. 2004; 200: 1197-203.
15. Clausen TM, Christoffersen S, Dahlbäck M, Langkilde AE, Jensen KE, Resende M, et al. Structural and functional insight into how the *Plasmodium falciparum* VAR2CSA protein mediates binding to chondroitin sulfate A in placental malaria. *J Biol Chem*. 2012; 287: 23332-45.
16. Dahlbäck M, Jørgensen LM, Nielsen MA, Clausen TM, Ditlev SB, Resende M, et al. The chondroitin sulfate A-binding site of the VAR2CSA protein involves multiple N-terminal domains. *J Biol Chem*. 2011; 286: 15908-17.
17. Resende M, Nielsen MA, Dahlbäck M, Ditlev SB, Andersen P, Sander AF, et al. Identification of glycosaminoglycan binding regions in the *Plasmodium falciparum* encoded placental sequestration ligand, VAR2CSA. *Malar J*. 2008; 7: 104.
18. Farley JH, Heathcock RB, Branch W, Larsen W, Homas D. Treatment of metastatic gestational choriocarcinoma with oral methotrexate in a combat environment. *Obstet Gynecol*. 2005; 105: 1250-4.
19. Hsu JY, Chen L, Gumer AR, Tergas AI, Hou JY, Burke WM, et al. Disparities in the management of ectopic pregnancy. *Am J Obstet Gynecol*. 2017; 217: 49.e1-e10.
20. Kawamura K, Kawamura N, Kumazawa Y, Kumagai J, Fujimoto T, Tanaka T. Brain-derived neurotrophic factor/tyrosine kinase B signaling regulates human trophoblast growth in an in vivo animal model of ectopic pregnancy. *Endocrinology*. 2011; 152: 1090-100.
21. Fan X, Rai A, Kambham N, Sung JF, Singh N, Petitt M, et al. Endometrial VEGF induces placental sFLT1 and leads to pregnancy complications. *J Clin Invest*. 2014; 124: 4941-52.
22. Fan X, Krieg S, Kuo CJ, Wiegand SJ, Rabinovitch M, Druzin ML, et al. VEGF blockade inhibits angiogenesis and reepithelialization of endometrium. *FASEB J*. 2008; 22: 3571-80.
23. Maynard SE, Min J-Y, Merchan J, Lim K-H, Li J, Mondal S, et al. Excess placental soluble fms-like tyrosine kinase 1 (sFlt1) may contribute to endothelial dysfunction, hypertension, and proteinuria in preeclampsia. *J Clin Invest*. 2003; 111: 649-58.
24. Gao K, Jiang X. Influence of particle size on transport of methotrexate across blood brain barrier by polysorbate 80-coated polybutylcyanoacrylate nanoparticles. *Int J Pharm*. 2006; 310: 213-9.
25. Campoli M, Ferrone S, Wang X. Functional and clinical relevance of chondroitin sulfate proteoglycan 4. *Adv Cancer Res*. 2010; 109: 73-121.
26. Akirav C, Lu Y, Mu J, Qu D, Zhou Y, Slevin J, et al. Ultrasonic detection and developmental changes in calcification of the placenta during normal pregnancy in mice. *Placenta*. 2005; 26: 129-37.
27. Lane LA, Qian X, Smith AM, Nie S. Physical chemistry of nanomedicine: understanding the complex behaviors of nanoparticles in vivo. *Annu Rev Phys Chem*. 2015; 66: 521-47.
28. van der Aa EM, Peereboom-Stegeman JH, Noordhoek J, Gribnau FW, Russel FG. Mechanisms of drug transfer across the human placenta. *Pharm World Sci*. 1998; 20: 139-48.
29. Ragelle H, Danhier F, Pr at V, Langer R, Anderson DG. Nanoparticle-based drug delivery systems: a commercial and regulatory outlook as the field matures. *Expert Opin Drug Deliv*. 2017; 14: 851-64.
30. Barenholz YC. Doxil®—the first FDA-approved nano-drug: lessons learned. *J Control Release*. 2012; 160: 117-34.
31. Takemoto K, Kanazawa K. AmBisome: relationship between the pharmacokinetic characteristics acquired by liposomal formulation and safety/efficacy. *J Liposome Res*. 2017; 27: 186-94.

32. Muoth C, Aengenheister L, Kucki M, Wick P, Buerki-Thurnherr T. Nanoparticle transport across the placental barrier: pushing the field forward! *Nanomedicine (Lond)*. 2016; 11: 941-57.
33. Lonner JH, Scuderi GR, Lieberman JR. Potential utility of liposome bupivacaine in orthopedic surgery. *Am J Orthop (Belle Mead NJ)*. 2015; 44: 111-7.
34. Ferrari M. Cancer nanotechnology: opportunities and challenges. *Nat Rev Cancer*. 2005; 5: 161-71.
35. Bajoria R, Contractor SF. Effect of surface charge of small unilamellar liposomes on uptake and transfer of carboxyfluorescein across the perfused human term placenta. *Pediatr Res*. 1997; 42: 520-7.
36. Bajoria R, Contractor SF. Effect of the size of liposomes on the transfer and uptake of carboxyfluorescein by the perfused human term placenta. *J Pharm Pharmacol*. 1997; 49: 675-81.
37. Barzago MM, Bortolotti A, Stellari FF, Diomede L, Algeri M, Efrati S, et al. Placental transfer of valproic acid after liposome encapsulation during in vitro human placenta perfusion. *J Pharmacol Exp Ther*. 1996; 277: 79-86.
38. Kaitu'u-Lino TuJ, Pattison S, Ye L, Tuohey L, Sluka P, MacDiarmid J, et al. Targeted nanoparticle delivery of doxorubicin into placental tissues to treat ectopic pregnancies. *Endocrinology*. 2013; 154: 911-9.
39. King A, Ndifon C, Lui S, Widdows K, Kotamraju VR, Agemy L, et al. Tumor-homing peptides as tools for targeted delivery of payloads to the placenta. *Sci Adv*. 2016; 2: e1600349.
40. Beards F, Jones LE, Charnock J, Forbes K, Harris LK. Placental Homing Peptide-microRNA Inhibitor Conjugates for Targeted Enhancement of Intrinsic Placental Growth Signaling. *Theranostics*. 2017; 7: 2940-55.
41. Cureton N, Korotkova I, Baker B, Greenwood S, Wareing M, Kotamraju VR, et al. Selective Targeting of a Novel Vasodilator to the Uterine Vasculature to Treat Impaired Uteroplacental Perfusion in Pregnancy. *Theranostics*. 2017; 7: 3715-31.
42. Wathes DC, Borwick SC, Timmons PM, Leung ST, Thornton S. Oxytocin receptor expression in human term and preterm gestational tissues prior to and following the onset of labour. *J Endocrinol*. 1999; 161: 143-51.
43. Adan RA, Van Leeuwen FW, Sonnemans MA, Brouns M, Hoffman G, Verbalis JG, et al. Rat oxytocin receptor in brain, pituitary, mammary gland, and uterus: partial sequence and immunocytochemical localization. *Endocrinology*. 1995; 136: 4022-8.
44. Paul JW, Hua S, Ilicic M, Tolosa JM, Butler T, Robertson S, et al. Drug delivery to the human and mouse uterus using immunoliposomes targeted to the oxytocin receptor. *Am J Obstet Gynecol*. 2017; 216: 283.e1-e14.
45. Refuerzo JS, Leonard F, Bulayeva N, Gorenstein D, Chiossi G, Ontiveros A, et al. Uterus-targeted liposomes for preterm labor management: studies in pregnant mice. *Sci Rep*. 2016; 6: 34710.
46. Keelan JA, Leong JW, Ho D, Iyer KS. Therapeutic and safety considerations of nanoparticle-mediated drug delivery in pregnancy. *Nanomedicine (Lond)*. 2015; 10: 2229-47.
47. Fried M, Duffy PE. Adherence of *Plasmodium falciparum* to chondroitin sulfate A in the human placenta. *Science*. 1996; 272: 1502-4.
48. Salanti A, Clausen TM, Agerbæk MØ, Al Nakouzi N, Dahlbäck M, Oo HZ, et al. Targeting human cancer by a glycosaminoglycan binding malaria protein. *Cancer cell*. 2015; 28: 500-14.
49. Oyston C, Stanley JL, Oliver MH, Bloomfield FH, Baker PN. Maternal Administration of Sildenafil Citrate Alters Fetal and Placental Growth and Fetal-Placental Vascular Resistance in the Growth-Restricted Ovine Fetus. *Hypertension*. 2016; 68: 760-7.
50. von Dadelszen P, Dwinnell S, Magee LA, Carleton BC, Gruslin A, Lee B, et al. Sildenafil citrate therapy for severe early-onset intrauterine growth restriction. *BJOG*. 2011; 118: 624-8.